Vol. 6, No. 3, June 2022, pp. 288-296

Current Optics and Photonics

Regular Paper

Optical Signal Sampling Based on Compressive Sensing with Adjustable Compression Ratio

Hongbo Zhou, Runcheng Li, and Hao Chi*

School of Communication Engineering, Hangzhou Dianzi University, Hangzhou 310018, China

(Received February 15, 2022 : revised April 5, 2022 : accepted April 22, 2022)

We propose and experimentally demonstrate a novel photonic compressive sensing (CS) scheme for acquiring sparse radio frequency signals with adjustable compression ratio in this paper. The sparse signal to be measured and a pseudo-random binary sequence are modulated on consecutively connected chirped pulses. The modulated pulses are compressed into short pulses after propagating through a dispersive element. A programmable optical filter based on spatial light modulator is used to realize spectral segmentation and demultiplexing. After spectral segmentation, the compressed pulses are transformed into several sub-pulses and each of them corresponds to a measurement in CS. The major advantage of the proposed scheme lies in its adjustable compression ratio, which enables the system adaptive to the sparse signals with variable sparsity levels and bandwidths. Experimental demonstration and further simulation results are presented to verify the feasibility and potential of the approach.

Keywords : Compressive sensing, Pulse stretch and compression; Sparse signals
OCIS codes : (060.2330) Fiber optics communications; (060.2360) Fiber optics links and subsystems

I. INTRODUCTION

Compressive sensing (CS) has attracted much research interest owing to its promising applications in the acquisition of wideband signals [1, 2]. CS offers an effective way to capture a sparse signal by using a digitizer with a sampling rate much lower than the Nyquist rate. The implementation of CS usually includes a measurement process and a reconstruction process. In the measurement process, the sparse signal of interest is mapped linearly into a few data points. With the measured data points, the sparse signal can be reconstructed by using an optimization method in the reconstruction process. Random demodulator (RD) and modulated wideband converter (MWC) are two well-established CS models for the acquisition of time-domain signals [3, 4]. Both of them involve the stages of mixing of the sparse signal with a pseudo-random binary sequence (PRBS), low-pass filtering and sub-sampling. Due to the advantage of large bandwidth offered by photonic techniques and devices, photonics-enabled CS is believed to be a potential solution to digital receiving of ultra-wideband sparse signals. For example, images can be recovered with the received light intensity and spatially illuminating patterns in single pixel-imaging and radar echo can be received without down-conversion in an MWC-based CS system [5, 6]. Up to now, many photonic CS schemes have been reported [7–20].

Valley *et al*. [7] initially demonstrated implementation of photonic CS measurement , in which a pulsed laser source and a spectral shaper based on spatial light modulator (SLM) were utilized to realize the mixing between a sparse RF signal and a PRBS in the optical domain. In [8], the measurement process of CS in a photonic link was reported, in which the optical mixing was realized based on the use of a continuous-wave (CW) source and an electro-optic modulator (EOM). Basis mismatch in the CS based on a photonic link has been investigated in [9]. Combination of the photonic CS with the technique of photonic time stretch was

*Corresponding author: chihao@hdu.edu.cn, ORCID 0000-0001-5913-2794

Color versions of one or more of the figures in this paper are available online.

pISSN: 2508-7266 / eISSN: 2508-7274 https://doi.org/10.3807/COPP.2022.6.3.288

proposed in [10] in order to further decrease the required sampling rate for capturing an ultra-wideband signal. Some approaches to implementing the function of low-pass filtering, that is necessary in CS, in the optical domain have been demonstrated successfully in [11, 12]. Some photonic multi-channel CS schemes based on MWC were reported in [13–15]. In [16], a photonic CS system using nanophotonic structures was proposed for spectral analysis, in which the randomness in the spectral responses of nanostructures was employed. A theoretical framework for the SLM-based photonic CS was given in [17]. Our recent work showed that the performance the SLM-based photonic CS can be greatly improved by using complementary outputs to realize an equivalent bipolar PRBS [18].

In [19, 20], a photonic CS scheme with the help of pulse stretch and compression were demonstrated. In their scheme, the sparse RF signal to be measured and the PRBS are modulated on dispersively stretched and chirped pulses; the pulse compression by propagating through a conjugate dispersive element with an opposite dispersion sign is to obtain the integral value (or the result of low-pass filtering) of the mixed signal, which eliminates the use of a low-pass filter or an integrator. In addition, by the process of pulse compression, a high signal-to-noise ratio (SNR) measurement can be achieved. In the scheme, each compressed pulse corresponds to a sample to be digitized and the sampling rate of the digitizer is determined by the pulse repetition rate of the applied pulsed laser. It is known in an RD-based CS system, the sampling rate R necessary to recover an input sparse signal depends on the Nyquist rate W and the sparsity level K of the input sparse signal, which can be given by an empirical rule as $R \approx 1.7\,K \log(W/K + 1)$ [2]. Considering the sparsity of input signals are unknown, it is highly desired to design a photonic CS system with adjustable sampling rate R or compression ratio W/R, adapting for different situations and ensuring the signal reconstruction. To our knowledge, there is no research reported on adjustable compression ratio in the field of photonic CS for wideband signal acquisition.

In this paper, we present a novel photonic CS scheme based on pulse stretch and compression for acquisition of continuous-time wideband signals with adjustable compression ratio. The sparse signal under test and PRBS are modulated on consecutively connected chirped pulses via EOMs. Next, the modulated pulses are time-compressed into a short pulse after propagating through a dispersive element and then sent into a programmable optical filter (POF) based on a SLM. Within the POF, the spectrum of compressed pulses is divided into several segments and each segment of the spectrum is sent to a corresponding output port. Due to the spectrum segmentation, each compressed pulse is transformed to a number of parallel subpulses and each of them corresponds to a sampling point. Therefore, the number of samples of each pulse from the pulsed laser can be greater than one, which depends on the number of spectral segments and is adjustable due to the use of POF. The major novelty of the proposed scheme lies in its adjustable compression ratio in photonic CS for wideband signal acquisition. By adjusting the number of spectral segments and output ports in POF, the proposed system can be adaptive to the sparse radio frequency signals with different sparsity levels and bandwidths. Theoretical analysis, numerical simulations and experimental demonstration are presented to verify the feasibility and potential of the approach.

II. PRINCIPLE

The schematic diagram of the proposed photonic CS scheme with adjustable compression ratio is shown in Fig. 1. The system consists of a mode-locked laser (MLL) for pulse generation, two EOMs for the modulation of sparse signal and PRBS, a pulse pattern generator (PPG) for generating PRBS, a spool of dispersion compensating fiber (DCF) and a spool of standard single-mode fiber (SSMF) before and after the EOMs respectively, a POF for spectrum slicing and demultiplexing, a number of photodetectors (PDs) with each PD corresponding to an output port of the POF for O/E conversion. Note that the DCF and SSMF modules have the same dispersion amount, but the opposite dispersion sign, which are used to implement the pulse stretching and compression.

The short pulses emitted from the MLL are broadened in time and get chirped after propagating through the DCF module. By setting the appropriate spectral width using the POF, each stretched pulse after the DCF module has a temporal width equal to the pulse repetition period, such that the pulses are connected with each other end to end. Therefore, the time-stretched pulses can be viewed as a continuous carrier. A sparse signal to be measured is modulated on the stretched pulses via the first EOM and then the modulated pulses are further modulated by a preset PRBS from the PPG at the second EOM. In this way, the mixing between the signal and the PRBS is realized. After the optical mixing, the pulses propagate through the SSMF module, which leads to a pulse compression. The compressed pulses are then incident into the SLM-based POF, in which the spectrum of pulses is divided into a number of segments and demultiplexed into different ports, in which each output port corresponds to a spectrum segment. Due to the property of frequency-to-time mapping (FTTM) of chirped pulses, each spectral segment corresponds to a time duration of a chirped pulse carrying the sparse signal and PRBS. The compressed pulses from the output ports of the POF are sent to PDs for O/E conversion. The pulses are captured by the following digitizers, which are utilized for reconstructing the sparse signal in a digital signal processing module.

The proposed CS scheme is based on the framework of RD [3]. The measurement process is modeled as: $\mathbf{y} = \mathbf{\Psi x} = \mathbf{DHRx}$, where $\mathbf{x}$ is an $N \times 1$ vector and denotes the sparse signal at or above Nyquist rate, $\mathbf{\Psi}$ is an $M \times N$ measurement matrix, $\mathbf{y}$ is an $M \times 1$ ($M \ll N$) vector and represents

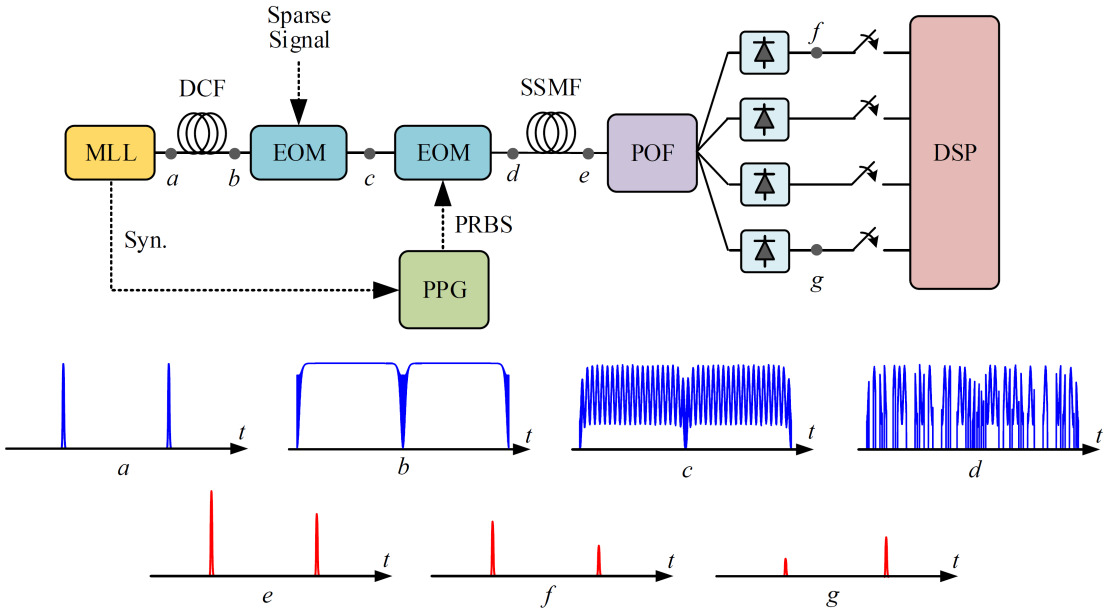

FIG. 1. Schematic diagram of the photonic compressive sensing (CS) with adjustable compression ratio. MLL, mode-locked laser; DCF, dispersion compensating fiber; EOM, electronic-optic modulator; PPG, pulse pattern generator; PRBS, pseudo-random bit sequence; SSMF, standard single-mode fiber; POF, programmable optical filter; PD, photodetector; DSP, digital signal processing. (a) The pulses emitted from MLL, (b) the broadened pulses after propagating through the DCF module, (c) the waveform of pulses after signal modulation, (d) The waveform of pulses after PRBS modulation, (e) the compressed pulses after propagating through SSMF, (f) the generated sub-pulses after POF segmentation, and (g) the generated sub-pulses after POF segmentation.

the measurement results, **R** is an $N \times N$ matrix and denotes the PRBS, **H** is an $N \times N$ matrix and denotes a low-pass filtering process, and **D** is an $M \times N$ matrix and denotes a sub-sampling process implemented by the digitizers. In the low-pass filtering process which is accomplished by an integrator, the mixed signal is accumulated in a time period of N/M bits. It has been proven theoretically and experimentally that the physical pulse compression is equivalent to an integrating process and the pulse peak value equals the integral result, which is also the basis of the pulse compression in CS [19, 21].

If $g_0(t)$ denotes the pulse emitted from the MLL and the dispersion values of the two dispersive elements are $\ddot{\Phi}$ and $-\ddot{\Phi}$ respectively, the pulse $g_1(t)$ after propagating through the first dispersive element can be expressed as

$$g_1(t) = g_0(t) * \frac{1}{\sqrt{j2\pi\ddot{\Phi}}} \exp\left(j\frac{t^2}{2\ddot{\Phi}}\right), \tag{1}$$

where * denotes the convolution operation, and $1/\sqrt{j2\pi\ddot{\Phi}}\exp[j(t^2/2\ddot{\Phi})]$ is the impulse response function of the first dispersive element. According to the property of the FTTM, the spectrum of the incident pulse is mapped to the time-domain waveform of the output pulse with the relationship of $\omega = t/\ddot{\Phi}$, which is: $g_1(t) = C \cdot \exp\left(j\frac{t^2}{2\ddot{\Phi}}\right) \cdot G_0(\omega)\Big|_{\omega=t/\ddot{\Phi}}$, where $G_0(\omega)$ denotes the spectrum of $g_0(t)$ and C denotes a constant. Therefore, after the modulation of the signal $x(t)$ and the PRBS $r(t)$, the modulated pulse $g'(t)$ can be expressed as

$$\begin{aligned} g_1'(t) &= C \cdot \exp\left(j\frac{t^2}{2\ddot{\Phi}}\right) \cdot G_0(t) \cdot x(t) \cdot r(t) \\ &= C \cdot \exp\left(j\frac{t^2}{2\ddot{\Phi}}\right) \cdot m(t), \end{aligned} \tag{2}$$

where $m(t) = G_0(t) \cdot x(t) \cdot r(t)$ denotes the waveform of the stretched and modulated pulse. After the second dispersive element, the waveform of the compressed pulse can be written as

$$\begin{aligned} g_2(t) &= g_1'(t) * \frac{1}{\sqrt{-j2\pi\ddot{\Phi}}} \exp\left(-j\frac{t^2}{2\ddot{\Phi}}\right) \\ &= \frac{1}{\sqrt{-j2\pi\ddot{\Phi}}} \int_{-\infty}^{+\infty} g_1'(\tau) \exp\left(-j\frac{(t-\tau)^2}{2\ddot{\Phi}}\right) d\tau \\ &= C' \cdot \int_{-\infty}^{+\infty} m(\tau) \cdot \exp\left(j\frac{t\tau}{\ddot{\Phi}}\right) d\tau = C' \cdot \mathfrak{F}^{-1}\{m(t)\}\Big|_{\omega=t/\ddot{\Phi}}, \end{aligned} \tag{3}$$

where C' denotes a constant and $1/\sqrt{-j2\pi\ddot{\Phi}}\exp[-j(t^2/2\ddot{\Phi})]$ is the impulse response of the second dispersive element. It is seen that the time-domain waveform of the compressed pulse is proportional to the inverse Fourier transform of the modulated pulse $m(t)$. Considering the limited bandwidth of the pulse, the compressed pulse $g_2(t)$ can be more exactly expressed as

$$g_2(t) = C' \cdot \int_{T_s}^{T_e} m(\tau) \cdot \exp\left(j\frac{t\tau}{\ddot{\Phi}}\right) d\tau, \tag{4}$$

where $T_x = \ddot{\Phi} \cdot \omega_x$ denotes the time point along the stretched/

chirped pulse corresponding to the angular frequency ω_x, and the start and stop times T_s and T_e correspond to the start and stop frequencies ω_s and ω_e of the pulses, respectively. Therefore, it can be seen that the peak value of the compressed pulse $g_2(0)=C'\cdot\int_{T_s}^{T_e} m(\tau)d\tau$ equals the integral value of $m(t)$ within the total time duration of the stretched pulse. In other words, the mixed product between the sparse signal $x(t)$ and the PRBS $r(t)$ within each pulse is accumulated as a single data point. The compression ratio of CS equals to the sequence length of PRBS within the time duration of a single stretched pulse. However, in real applications, it is highly desired that the compression ratio or the sampling rate can be adjustable since the sparsity level of input signals may vary, as the sampling rate necessary to recover sparse signals should follow an empirical rule $R \approx 1.7\ K \log(W / K + 1)$, where R is the sampling rate, W is the Nyquist rate, and K is the sparsity level.

In this work, we propose to use an SLM-based POF to realize adjustable compression ratio. After passing the POF, the spectrum of pulses is divided into several segments and demultiplexed into different output ports. Each spectral segment corresponds to a time duration of a chirped pulse carrying the sparse signal and PRBS. Therefore, the compression ratio is equal to the number of spectral segments. The optical pulses from the output ports can be expressed as

$$\begin{aligned} s_1(t) &= C'\int_{T_s}^{T_1} m(\tau)\cdot\exp(j\frac{t\tau}{\ddot{\Phi}})d\tau \\ s_2(t) &= C'\int_{T_1}^{T_2} m(\tau)\cdot\exp(j\frac{t\tau}{\ddot{\Phi}})d\tau \\ &\vdots \\ s_n(t) &= C'\int_{T_{n-1}}^{T_e} m(\tau)\cdot\exp(j\frac{t\tau}{\ddot{\Phi}})d\tau, \end{aligned} \tag{5}$$

where ω_1, ω_2, ... are boundaries of spectral segments, as shown in Fig. 2. It should be noted that the peak value of the above pulse $s_i(0)$ is the accumulation of the mixed signal within the time range sliced by the POF. Benefiting from that, the original compressed pulse are changed to be n pulses, which means the compression ratio is decreased by a factor $1/n$.

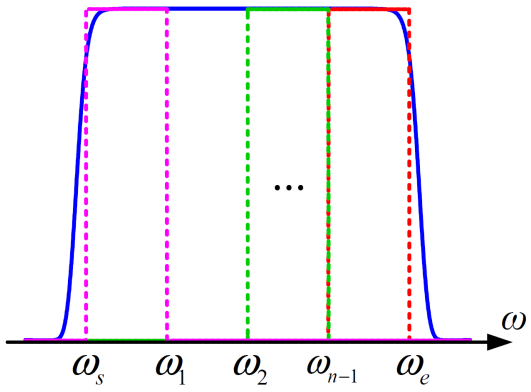

FIG. 2. Illustration of the spectral segmentation: (solid) the spectrum of original pulse; (dotted) the passbands of spectral segments.

III. RESULTS AND DISCUSSIONS

3.1. Experimental Setup

A proof-of-concept experiment with the setup as shown in Fig. 1 was implemented to demonstrate the proposed approach. A passive MLL (ELMO; Menlo Systems Inc., Martinsried, Germany)with repetition rate of 100 MHz was employed to generate short pulses. The output power from the MLL was around 13.5 dBm. A DCF module and a 20-km SSMF module with dispersion values of +424 ps^2 and −424 ps^2 respectively were used as the dispersive elements. Microwave signals generated from a signal generator (R&S SMB 100A; Rohde & Schwarz Inc., München, Germany) and a vector network analyzer (R&S ZNB 40; Rohde & Schwarz Inc., München, Germany) were applied to a 40-GHz Mach-Zehnder modulator (MZM) (KG-AMBOX-15-40-PP-FA; Conquer Photonics Co. Ltd., Beijing, China), which had an insertion loss of about 7 dB. A PRBS pattern, generated from a PPG (MP2100B, Anritsu, Kanagawa, Japan) was applied to the second MZM (MU-AM-15-20-PS-FA; Conquer Photonics Co. Ltd., Beijing, China). Note that the PPG was synchronized with the MLL via the trigger-in port. A POF with an insertion loss of 4.5 dB (WS 4000A; Finisar, CA, USA) was employed to segment the spectrum into two to four parts in a total bandwidth of 29 nm, in which each output port corresponded to a spectral segment. The output pulses from the POF were received by PDs with a bandwidth of 10 GHz. The received signal was recorded by a four-port real-time oscilloscope (R&S RTP084; Rohde & Schwarz Inc., München, Germany) with a bandwidth of 8 GHz and a sampling rate of 20 GHz.

Figure 3 shows typical experimental waveforms recorded by the oscilloscope. Figure 3(a) is the stretched pulses modulated by a 1-GHz single-tone signal, in which the pulses are almost consecutively connected. The time duration of each stretched pulse was around 9.68 ns, which was close to the pulse interval of 10 ns. In Fig. 3(b), the modulated stretched pulses further mixed with a 2.4-Gb/s PRBS is shown. Figure 3(c) is the compressed pulses after the second dispersive element without any spectral segmentation. Figure 3(d) is the compressed pulses after spectral segmentation from one of the two output ports of the POF. Note that after spectral segmentation, each compressed pulse in Fig. 3(c) was converted into two parallel sub-pulses as in Figs. 3(d) and 3(e) and the repetition rate of sub-pulses is the same as the input pulse source. The transmission spectra set in POF with two and three spectral segments are shown in Figs. 4(a) and 4(b). It should be noted that the fluctuation in the transmission spectra is introduced to compensate for the uneven spectrum of the employed MLL, which is shown in Fig. 4(c). As a result of the fluctuation compensa-

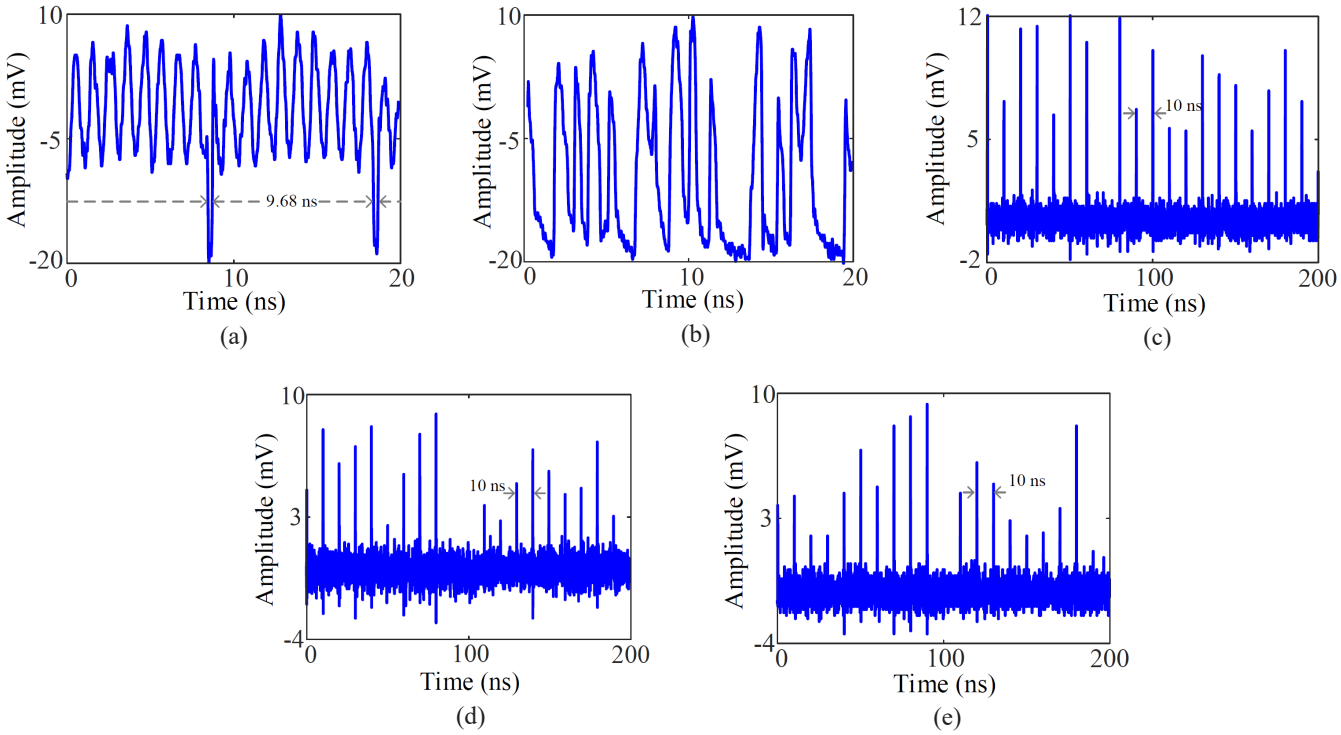

FIG. 3. Experimental waveforms recorded by the oscilloscope. (a) The pulses after signal modulation, (b) the pulses after PRBS modulation, (c) the compressed pulses without spectral segmentation, (d) and (e) the compressed pulses with spectral segmentation from two output ports.

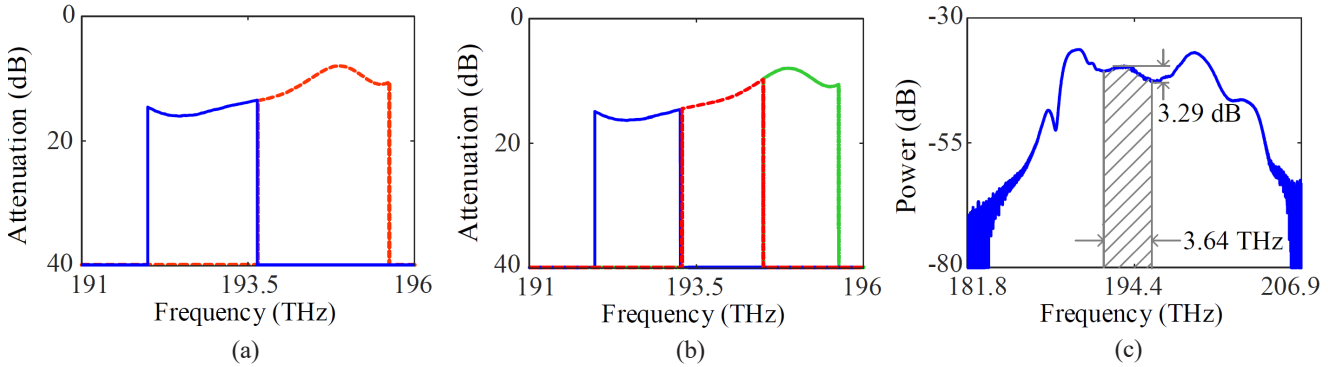

FIG. 4. Transmission spectra set in the programmable optical filter (POF) with (a) two spectral segments, (b) three spectral segments, and (c) the spectrum of the applied mode-locked laser (MLL).

tion, the output spectrum is almost flat and the fluctuation is less than 0.7 dB, which is shown in Fig. 5.

3.2. Experiment Results

We firstly studied the photonic CS system without spectral segmentation. In this case, each input pulse corresponded to an output pulse. Set by using the POF, the effective optical bandwidth of optical pulses was 29 nm, centered at 1547 nm. The rate of the PRBS from the pattern generator was set as the Nyquist rate of the system, *e.g.* 2.4 Gb/s, and the length of PRBS was set as 1200 bits. Therefore, the system bandwidth of the CS system was 1.2 GHz. Since the

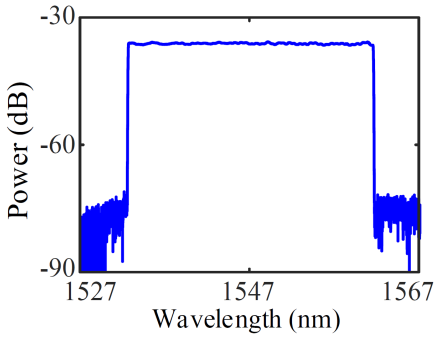

FIG. 5. Output spectrum from the programmable optical filter (POF) without spectral segmentation.

repetition rate of the MLL is 100 MHz, the 1200-bit PRBS covered 50 consecutive pulses and each pulse was covered by 24 bits of the PRBS. Therefore, the compression ratio of this CS system was 24. Since the spectrally sparse signals were common and easy to generate, we selected the spectrally sparse signals to test the proposed system. A single-tone signal with a frequency of 970 MHz and a two-tone signal with frequencies of 720 MHz and 970 MHz were applied to the system, one after another. In the input two-tone signal, the powers of two tones are equal. The output pulses were captured by the oscilloscope, which were then processed by an off-line program. In the program, the reconstruction algorithm *l*1-ls, developed by Kim *et al*. [22], was employed to recover the input sparse signal. First, the recovered spectra without spectral segmentation are shown in Figs. 6(a) and 6(b). Due to the high compression ratio (insufficient measurements), the spectral recovery was not good, which can be seen from the results.

Next, we used the POF to slice the spectrum into two segments, with the transmission spectrum as shown in Fig. 4(a), and the two spectral parts were sent to different ports. Due to the property of FTTM, the segmentation in the frequency domain means the segmentation in the time domain. Therefore, after the spectral segmentation, one pulse carrying 24-bit information was split into two sub-pulses with each carrying 12-bit information. Compared to the experiment without spectral segmentation, two measurements were obtained in each pulse repetition period and the compression ratio is thus halved to be 12. Again in this case, a single-tone signal with a frequency of 970 MHz and a two-tone signal with frequencies of 720 MHz and 970 MHz were applied to the system, one after the other. The reconstructed spectra were shown in Figs. 6(c) and 6(d), respectively. The single-tone signal and the two-tone signal were reconstructed successfully, which is due to the decreased compression ratio (or the increased number of measurements). It should be noted that due to the nonlinearity in the system (such as that in EOMs), an octave was considered in the experiment in order to exclude the impact of the second-order nonlinearity. The amplitude ratio between the two spectral components in the recovered two-tone signal is 1.3:1. Similarly, as long as the POF has more output ports, the compression ratio could be decreased further. The proposed scheme with three spectral segments and three outputs was also tested. In this case, there were three measurements in each pulse repetition period and the compression ratio was 8. The same single-tone and two-tone signals as in the previous two cases were applied. The recovered spectra are shown in Figs. 6(e) and 6(f). It is seen that the sparse signal is recovered successfully again. The amplitude ratio between the two spectral components in the recovered two-tone signal is around 0.8:1. It is noteworthy that the adjustment of compression ratio was achieved by changing the number of spectral segments and sub-channels. It should be noted that the case with high compression ratios had greater SNR in the experimental results. In the proposed scheme,

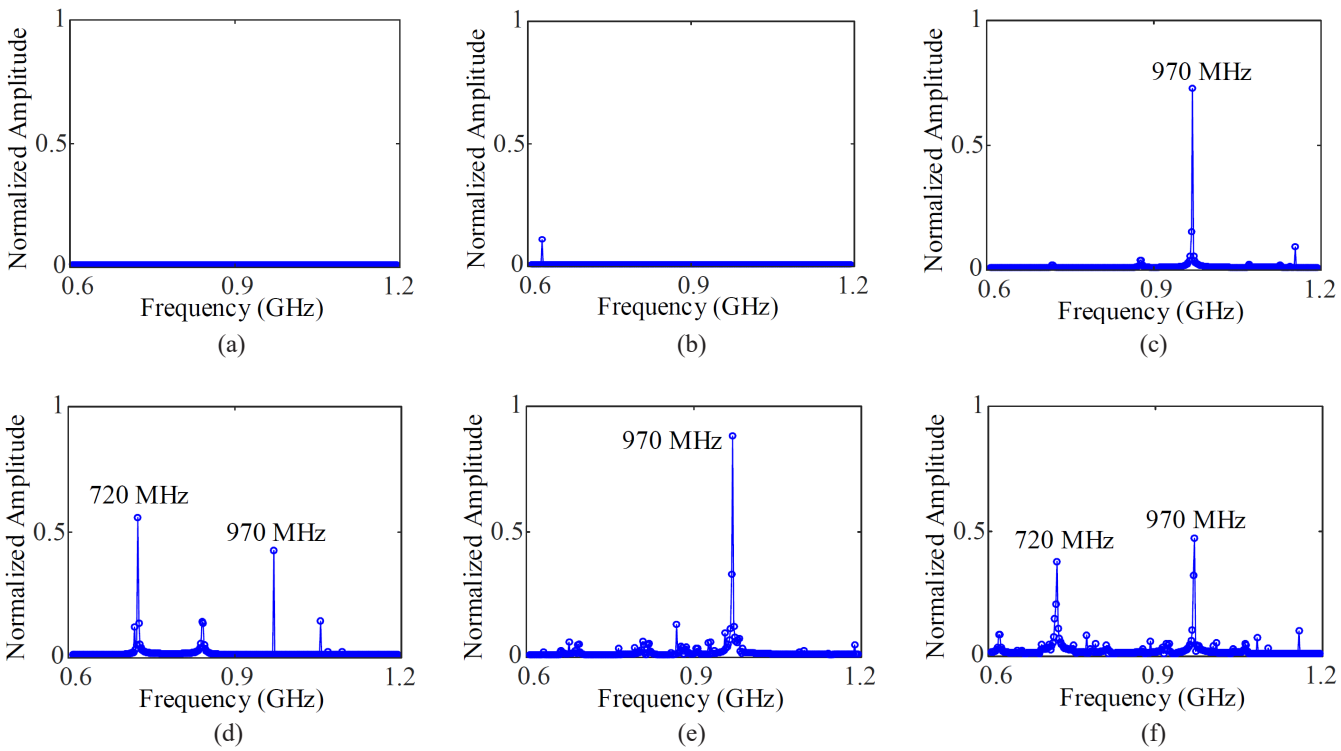

FIG. 6. The reconstructed spectra of single-tone signal and two-tone signal under different spectral segmentations. (a) and (b) are one spectral segment, compression ratio = 24, (c) and (d) are two spectral segments, compression ratio = 12, and (e) and (f) are three spectral segments, compression ratio = 8.

each spectral segment was mapped into a duration of time-domain waveform. With differing amounts of spectral segments and output ports, the proposed scheme could handle signals with different sparsity and realize different system bandwidths. Due to the non-ideal fringes in spectral segments in the experiment, more spectral segments brought more gaps between adjacent pulses, which influenced the signal splicing. As a result, a lower compression ratio led to better performance in spectral identification, but resulted in a lower SNR due to more spectral segments being involved in the experiment.

In order to improve the electrical bandwidth of the CS system to accommodate to the sparse signals with higher frequencies, PRBS with higher bit rate is necessary. In this case, more output ports had to be allocated, which helped to keep the compression ratio within an acceptable range. Therefore, additional simulations with more spectral segments were implemented to demonstrate the cases. The parameters of the optical system, such as the optical bandwidth, repetition rate, dispersion values, were set the same as the experimental system. The electrical bandwidth of the CS system was increased to be 2.4 GHz, which corresponds to a Nyquist rate of 4.8 Gb/s. The rate of PRBS was set as the Nyquist rate and the length of PRBS was set also to be 1200 bits. A two-tone signal with frequencies of 1.85 GHz and 2.1 GHz was applied to the system. In the input two-tone signal, the powers of two tones are equal. The recovered spectra are shown in Fig. 7, where Fig. 7(a) corresponds to the case that the number of spectral segments equals 4 and the compression ratio equals 12, Fig. 7(c) corresponds to the case that the number of spectral segments equals 6 and the compression ratio equals 8. The amplitude ratios between each frequency component are 1:1.2 and 1:1.4 respectively. It should be noted that the reconstructed frequency of 1.85 GHz is located at the frequency of 1.848 GHz actually. It can be explained by a basis mismatch, in which the resolution of reconstructed signal was restricted by the sparsity basis *e.g.* the DFT basis in this scheme [9]. In addition, a three-tone signal with frequencies of 1.44 GHz, 1.85 GHz and 2.1 GHz was applied to the modulator with 4 and 6 spectral segments, respectively. The powers of three tones were equal as well. The results are shown in Figs. 7(b) and 7(d). The figures show the reconstruction performance was pretty good for both the two-tone and three-tone signals, which also verifies the capability of adjustable compression ratio of the proposed approach. The amplitude ratios between each frequency component are 0.86:1:1 and 1.25:1:1.4 respectively.

In the experiment, the output spectrum of the applied MLL drifted with time, which influenced the mapped time waveforms. The dispersion mismatch between SSMF and DCF also had a negative impact on the system performance. Therefore, we studied the relationship of the SNR of the recovered signal on the dispersion difference between the first and second dispersive element using simulations. In the simulation, a single-tone signal (spectrally sparse) was

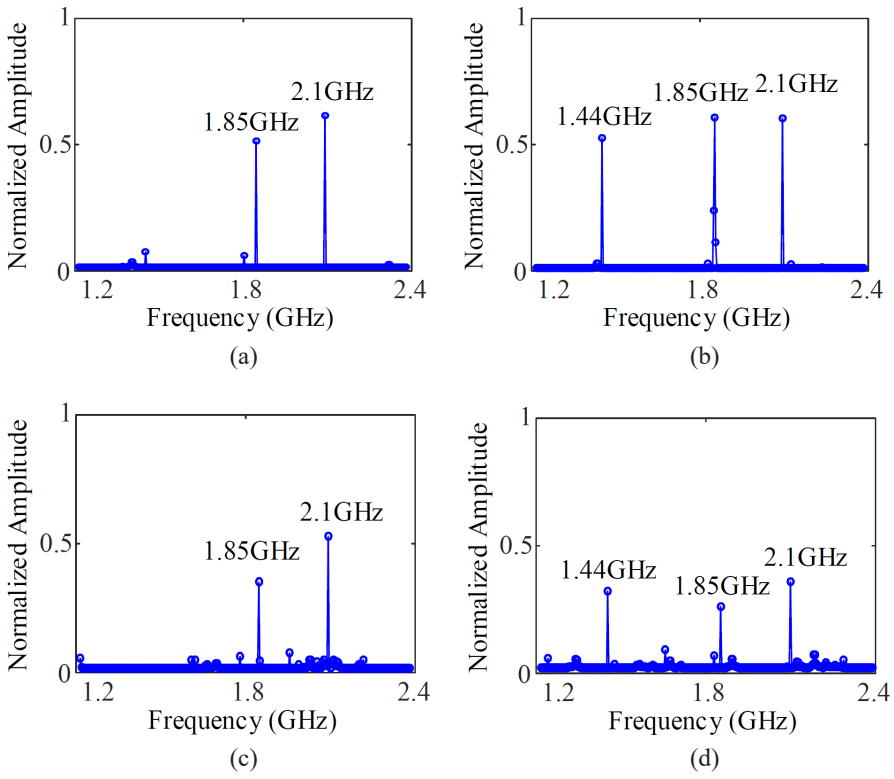

FIG. 7. The reconstructed spectra. (a) Two-tone signal, 4 spectral segments; (b) three-tone signal, 4 spectral segments; (c) two-tone signal, 6 spectral segments; (d) three-tone signal, 6 spectral segments.

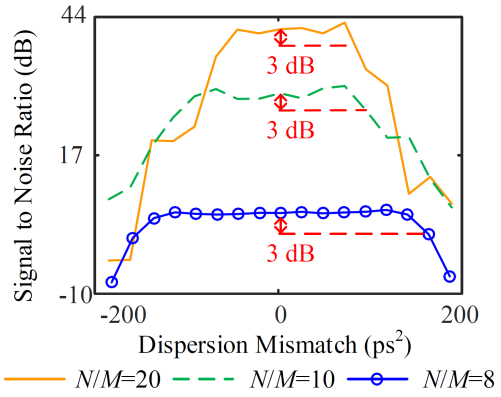

FIG. 8. SNR of the recovered signal vs. dispersion mismatch.

tested with different compression ratios, namely, 8, 10 and 20. The results are shown in Fig. 8. It can be seen that the SNR of the reconstructed signal degrades with the increase of dispersion difference. When compression ratio is 8, the impact induced by dispersion mismatch is relatively small, as more measurement results were used to reconstruct the signal. Under the compression ratios of 20, 10 and 8, the dispersion differences that resulted in a decrease of 3 dB in SNR were 80 ps^2, 80 ps^2 and 140 ps^2, respectively, which can be viewed as the tolerance on the dispersion mismatch.

The major advantage of the proposed scheme lies in the adjustable compression ratio achieved by using the POF. As analyzed in [21], the photonic CS schemes based on pulse stretch and compression had a compression ratio determined by the length of the PRBS within a pulse repetition period, which is decided by the system bandwidth. In many scenarios, the compression ratio was too high for a given system bandwidth and pulse repetition period to obtain a good sparse recovery. In our approach, the high compression ratio can be effectively reduced by using the POF, which largely improves the performance of the CS system in terms of recovery probability. The presented results verified the advantage of the approach. A major limitation of the approach lies in that the currently available POF had at most four outputs, which indicates that the compression ratio can be reduced by at most four times in the current experiments. Another issue we should point out is that the system configuration in Fig. 1 is somewhat similar to the real-time Fourier Transform system based on the technique of temporal pulse shaping [23], which also contains a pair of dispersive elements with opposite dispersion values. However, the two systems differ in the function and mechanism, despite that the given photonic CS system can also be used for frequency measurements [24–26].

In the future, photonic CS architectures with more output ports for acquiring signals with higher sparsity can be further investigated. The pulse compression and spectral segmentation proposed in this work can also be used in a photonic MWC architecture with multiple photonic links, which is capable of reconstructing wideband sparse signals [4].

IV. CONCLUSION

In summary, a novel photonic CS scheme for acquiring sparse radio frequency signals with adjustable compression ratio is presented. By means of programmable spectral segmentation, multiple and variable measurements per pulse can be realized, which leads to adjustable compression ratio of the proposed CS approach. The proposed approach largely alleviates the burden on signal recovery imposed by high compression ratio in the pulse-based photonic CS schemes and makes the system adaptive to the sparsity level and bandwidth of the input sparse signals. A full analytical model characterizing the proposed approach has been presented. A proof-of-concept experiment is implemented, which fully verifies the feasibility of the approach. Further numerical results are also presented to show the potential of the scheme.

FUNDING

National Natural Science Foundation of China (grant number: 61975048); Natural Science Foundation of Zhejiang Province (grant number: LZ20F010003).

DISCLOSURES

The authors declare no conflicts of interest.

DATA AVAILABILITY

Data underlying the results presented in this paper are not publicly available at the time of publication, which may be obtained from the authors upon reasonable request.

REFERENCES

1. E. J. Candes, J. Romberg, and T. Tao, "Robust uncertainty principles: exact signal reconstruction from highly incomplete frequency information," IEEE Trans. Inf. Theory **52**, 489–509 (2006).
2. J. A. Tropp, J. N. Laska, M. F. Duarte, J. K. Romberg, and R. G. Baraniuk, "Beyond Nyquist: efficient sampling of sparse bandlimited signals," IEEE Trans. Inf. Theory **56**, 520–544 (2010).
3. J. M. Nichols and F. Bucholtz, "Beating Nyquist with light: a compressively sampled photonic link," Opt. Express **19**, 7339–7348 (2011).
4. M. Mishali and Y. C. Eldar, "From theory to practice: sub-Nyquist sampling of sparse wideband analog signals," IEEE J. Sel. Top. Signal Process. **4**, 375–391 (2010).
5. R. G. Baraniuk, "Compressive sensing [Lecture notes]," IEEE Signal Process. Mag. **24**, 118–121 (2007).
6. Q. Guo, Y. Liang, M. Chen, H. Chen, and S. Xie, "Compressive spectrum sensing of radar pulses based on photonic techniques," Opt. Express **23**, 4517–4522 (2015).
7. G. C. Valley, G. A. Sefler, and T. J. Shaw, "Compressive sens-

ing of sparse radio frequency signals using optical mixing," Opt. Lett. **37**, 4675–4677 (2012).
8. L. Yan, Y. Dai, K. Xu, J. Wu, Y. Li, Y. Ji, and J. Lin, "Integrated multifrequency recognition and downconversion based on photonics-assisted compressive sampling," IEEE Photonics J. **4**, 664–670 (2012).
9. C. V. Mclaughlin, J. M. Nichols, and F. Bucholtz, "Basis mismatch in a compressively sampled photonic link," IEEE Photonics Technol. Lett. **25**, 2297–2300 (2013).
10. H. Chi, Y. Chen, Y. Mei, X. Jin, S. Zheng, X. Zhang, "Microwave spectrum sensing based on photonic time stretch and compressive sampling," Opt. Lett. **38**, 136–138 (2013).
11. Y. Chen, Y. Ding, Z. Zhu, H. Chi, S. Zheng, X. Zhang, X. Jin, M. Galili, and X. Yu, "Photonic compressive sensing with a micro-ring-resonator-based microwave photonic filter," Opt. Commun. **373**, 65–69 (2016).
12. Z. Zhu, H. Chi, T. Jin, S. Zheng, X. Yu, X. Jin, and X. Zhang, "Photonics-enabled compressive sensing with spectral encoding using an incoherent broadband source," Opt. Lett. **43**, 330–333 (2018).
13. H. Nan, Y. Gu, and H. Zhang, "Optical analog-to-digital conversion system based on compressive sampling," IEEE Photonics Technol. Lett. **23**, 67–69 (2011).
14. Y. Liang, M. Chen, H. Chen, C. Lei, P. Li, and S. Xie, "Photonic-assisted multi-channel compressive sampling based on effective time delay pattern," Opt. Express **21**, 25700–25707 (2013).
15. Q. Guo, Y. Liang, M. Chen, H. Chen, S. Yang, and S. Xie, "Time-interleaved 20-GHz modulated wideband converter based on random optical sampling," IEEE Photonics Technol. Lett. **27**, 1022–1025 (2015).
16. Z. Wang and Z. Yu, "Spectral analysis based on compressive sensing in nanophotonic structures," Opt. Express **22**, 25608–25614 (2014).
17. Z. Zhu, H. Chi, S. Zheng, T. Jin, X. Jin, and X. Zhang, "Analysis of compressive sensing with optical mixing using a spatial light modulator," Appl. Opt. **54**, 1894–1899 (2015).
18. H. Chi, H. Zhou, S. Yang, J. Ou, Y. Zhai, and B. Yang, "Compressive sensing based on optical mixing using a spectral shaper with bipolar coding," Opt. Express **29**, 16422–16431 (2021).
19. B. T. Bosworth and M. A. Foster, "High-speed ultrawideband photonically enabled compressed sensing of sparse radio frequency signals," Opt. Lett. **38**, 4892–4895 (2013).
20. B. T. Bosworth, J. R. Stroud, D. N. Tran, T. D. Tran, S. Chin, and M. A. Foster, "Ultrawideband compressed sensing of arbitrary multi-tone sparse radio frequencies using spectrally encoded ultrafast laser pulses," Opt. Lett. **40**, 3045–3048 (2015).
21. H. Chi and Z. Zhu, "Analytical model for photonic compressive sensing with pulse stretch and compression," IEEE Photonics J. **11**, 5500410 (2019).
22. S. Kim, K. Koh, M. Lustig, S. Boyd, and D. Gorinevsky, "An interior-point method for large-scale ℓ1-regularized least squares," IEEE J. Sel. Top. Signal Process. **1**, 606–617 (2007).
23. A. M. Weiner, "Femtosecond pulse shaping using spatial light modulators," Rev. Sci. Instrum. **71**, 1929–1960 (2000).
24. J. Yao and X. Zou, "An optical approach to microwave frequency measurement with adjustable measurement range and resolution," IEEE Photonics Technol. Lett. **20**, 1989–1991 (2008).
25. H. Chi, X. Zou, and J. Yao, "An approach to the measurement of microwave frequency based on optical power monitoring," IEEE Photonics Technol. Lett. **20**, 1249–1251 (2008).
26. X. Zou, W. Pan, B. Luo, and L. Yan, "Photonic approach for multiple-frequency-component measurement using spectrally sliced incoherent source," Opt. Lett. **35**, 438–440 (2010).